Development of Numerical Simulation to Predict the Microstructure and Temperature History of Wire Coil in the Stelmor Process

YING TSOU

Iron and Steel Research & Development Department
China Steel Corporation

This study developed a simulation tool by considering the transformation of material microstructure and release of latent heat to analyze the effects of insulation covers on heat transfer during the slow cooling process of coils. The main results include validating the developed tool with slow cooling experiments that achieved a maximum temperature history error of approximately 3%, meeting the requirement for engineering applications. Since the cooling rates vary at different sections, the simulation of tensile strength (TS) distribution along the wire coil showed a maximum difference (ΔTS) of 97 MPa. Furthermore, the radiative heat was found to dominate heat transfer during the cooling process constituting 75% and 88% of the total heat transfer at the central part and side part of the coils respectively. Future applications of the developed simulation tool aim to analyze the variations of wire coils in the Stelmor process and to enhance the quality of the product.

Keywords: Stelmor, Wire coils, Simulation

1. INTRODUCTION

During the Stelmor cooling process (as shown in Fig.1), the wire rod experiences uneven distribution due to staggered stacking, leading to areas of varying density. The wire rod at the sides is more densely packed. The difficulty in heat dissipation, results in slower cooling rates and the formation of hot spots. In contrast, the wire rod in the middle cools more efficiently due to better cooling conditions, resulting in faster cooling rates and the formation of cold spots. The cooling rate of the wire rod is closely related to its microstructure. Hot spots may form microstructures with lower tensile strength (TS), such as ferrite and pearlite, while cold spots may form microstructures with higher TS, such as ferrite, bainite, and pearlite. This results in significant TS variation within the wire rod coil.

In past studies, the cooling temperature history of wire rods has often been analyzed using simulation methods. Monserrat[1] established a phase transformation model for wire rods using the JMAK equation and simulated the cooling process using Fluent and UDF, with an experimental platform set up for verification. This approach achieved good predictive accuracy for the cooling temperature history of SAE1080 steel. Michal et al.[2] developed a phase transformation analysis tool for 32CrB4 steel using a modified JMAK equation, analyzing the microstructure under different cooling rates to adjust the Stelmor cooling conditions to achieve the target microstructure. Huang[3, 4] analyzed the flow field around the wire rod under blowing conditions through CFD analysis, finding that the cooling rates in the middle and inner edge of the wire rod were faster than in the center. Ring spacing was identified as a major factor affecting cooling rates; reducing ring spacing caused a sharp decrease in the edge cooling rate. Additionally, the largest deviations in cooling rates and mechanical properties occurred in the upper edge regions that cooled very slowly, especially when ring spacing was small. To address this, improvements such as increasing ring spacing, adjusting airflow nozzle direction, and optimizing deflectors were proposed.

In studies on improving cooling within the wire coil, Zhang Jun et al.[5] used high-speed airflow to create negative pressure, drawing water into nozzles for atomization, thereby enhancing the wire rod's cooling capability with mist cooling. This increased the qualification rate of curtain line steel products at Wuhan Iron and Steel from 87% to 95%. Huang[6] used CFD-assisted analysis to improve the temperature difference between hot and cold spots in the wire rod during rapid cooling, reducing the temperature difference between sparse and dense areas from 69.7℃ to 18.4℃ after installing deflectors below the wire rod. Additionally, CFD was used to analyze nozzle flow fields, optimizing jet effects by increasing nozzle gaps, and length, and reducing the

distance between nozzles and steel rollers, which improved the cooling rate by 17%.

Relevant patents include Hu Xiaodong et al.[7] installed a spray device above the conveyor belt, with fans below for bidirectional cooling of the wire rod, though uneven spraying could cause rust spots. Zhang Chi et al.[8] installed fans above the Stelmor conveyor belt in a suspended manner, blowing air diagonally onto the wire rod surface to increase cooling rates and uniformity. Zhou Min et al.[9] installed fans above the Stelmor conveyor belt with a duct having one inlet and two outlets, directing airflow to both sides of the wire rod to enhance hotspot cooling.

CFD simulations facilitate observing hotspots in the upper side and middle of the wire rod caused by airflow obstruction, aiding in enhancing cooling design to improve temperature uniformity. Literature has used the JMAK equation to simulate phase transformations and latent heat in wire rods, with simulation temperature distributions verified experimentally. These models are applied in this study. Besides, no research on the slow cooling mode of Stelmor covers or patents related to the optimization design of insulation covers was found. In this study, the cooling mechanism of slow cooling was investigated through simulations.

2. NUMERICAL METHOD

During the slow cooling process of wire coils under the insulation cover, the main heat dissipation mechanisms are radiation and convection due to relative motion (without fan-forced convection). In this study, a physical model is established and solved by using computational fluid dynamics (CFD). The cooling process of wire coils involves phase transformation and exothermic reactions simulated using the JMAK (Johnson Mehl Avrami Kolmogorov) equation coupled with flow field simulation.

This study focuses on wire coils with a diameter of 5.5 mm and a coil diameter of 1050 mm. The investigated region is shown in Fig.1. Assuming a symmetrical distribution of physical quantities on both sides, the computational domain is simplified to half of the original shape (Fig.2.) to enhance the efficiency of the simulation calculations.

Fig.1. Photo of the Stelmor process and insulation cover.

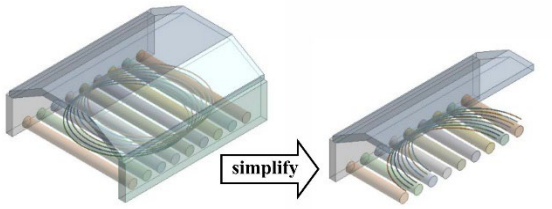

Fig.2. Geometric Model (Left: Original Geometry, Right: Simplified Geometry).

A physical model is established for the slow cooling phenomenon of wire coils during the Stelmor process. Under the assumptions of transient, incompressible flow, and Newtonian fluid, the governing equations are formulated as equations (1) to (3).

Here t、ρ、μ、$\varkappa$、$\vec{V}$、T represent time, density, viscosity coefficient, thermal conductivity, velocity vector, and temperature respectively [1]~[4].

$$\frac{D\rho}{Dt} + \rho\left(\nabla \cdot \vec{V}\right) = 0 \quad \text{.....(1)}$$

$$\rho \frac{D\vec{V}}{Dt} = -\nabla P + \mu \nabla^2 \vec{V} \quad \text{.....(2)}$$

$$\rho C_p \frac{DT}{Dt} = \nabla \cdot (k\nabla \mathrm{T}) + \mathrm{Q} \quad \text{.....(3)}$$

Where Q is the source term used to simulate the effects of heat absorption and release during phase transformation on the temperature distribution of the wire coil. The k– ϵ model is chosen to simulate the turbulence phenomenon. For radiation simulation, the radiation effect of the surrounding gas is not considered. The radiative heat transfer is related only to the relative positions of the spatial surfaces. Therefore, the S2S (Surface-to-Surface) model is selected under applied assumptions.

The microstructure of the wire coil undergoes phase transformation during the cooling process. Depending on the cooling rate, austenite may transform into ferrite (f), pearlite (p), bainite (b), and martensite (m). According to the literature[10], under the slow cooling conditions of the Stelmor process without air blowing, the cooling rate is below 2.5℃/s and the main phase transformations are from austenite to ferrite and pearlite. However, the cooling rate may exceed 10℃/s during rapid cooling and the bainite and martensite could be formed. The phase transformation process accompanied by the release of latent heat will affect the temperature distribution of the wire coil.

The phase transformation model adopts the Johnson-Mehl-Avrami-Kolmogorov (JMAK) equation to describe the volume fraction (X) of the phases generated by nucleation (f, p, b) and non-nucleation (m) transformations, as shown in equation (4). The relevant coefficients b and n are temperature (T) dependent.

$$\begin{cases} X_{f,p,b} = 1 - exp(-bt^n) \\ X_m = 1 - exp[-\alpha(Ms - T)] \end{cases} \quad \text{.....(4)}$$

The JMAK equation describes the S-curve of the phase transformation process. By rearranging the equation into form (5), it could be considered a linear equation. Where *n* is the slope and *ln(b)* is the intercept. Here $(X, t)_{Ta}$ represents the percentage of microstructure and time at a certain temperature (Ta). From the TTT diagram, the initial and final statuses can be defined as $(0.1\%, t_{0.1\%})_{Ta}$ and $(99.9\%, t_{99.9\%})_{Ta}$. Then the coefficients *n* and *b* at that temperature (Ta) can be determined.

$$ln[-ln(1-X)] = ln(b) + n \cdot ln(t) \text{ ..... (5)}$$

However, the timing of the phase transformation is simulated using the incubation time. When the accumulated incubation time f(t) exceeds 1, the phase transformation reaction is triggered. The incubation time τ_i is calculated from the start time of the phase transformation and the TTT curve. The released heat (Q) associated with the phase transformation process is calculated using equation (10), where the phase fraction and latent heat calculations are added to the time loop of the transient CFD solution process.

$$f(t) = \sum \frac{\Delta t}{\tau_i} \text{.....(6)}$$

$$Q = \Delta H \frac{\Delta X}{\Delta t} \text{.....(7)}$$

According to the results of a previous study[11]: There is a high linear correlation between the hardness (HV) of alloy steel and its tensile strength (TS). This relationship is expressed by equation (8). The hardness (HV) of different microstructures is related to the carbon content and undercooling. After calculating the microstructure, phase transformation temperature, and other information through numerical methods, the hardness of the wire rod can be determined using the rule of mixture. Then the TS distribution can be predicted from the hardness.

$$TS = -99.8 + (3.734)HV \text{.....(8)}$$

In the CFD solution process (Fig.3.), the real-time temperature distribution of the wire coil is captured in

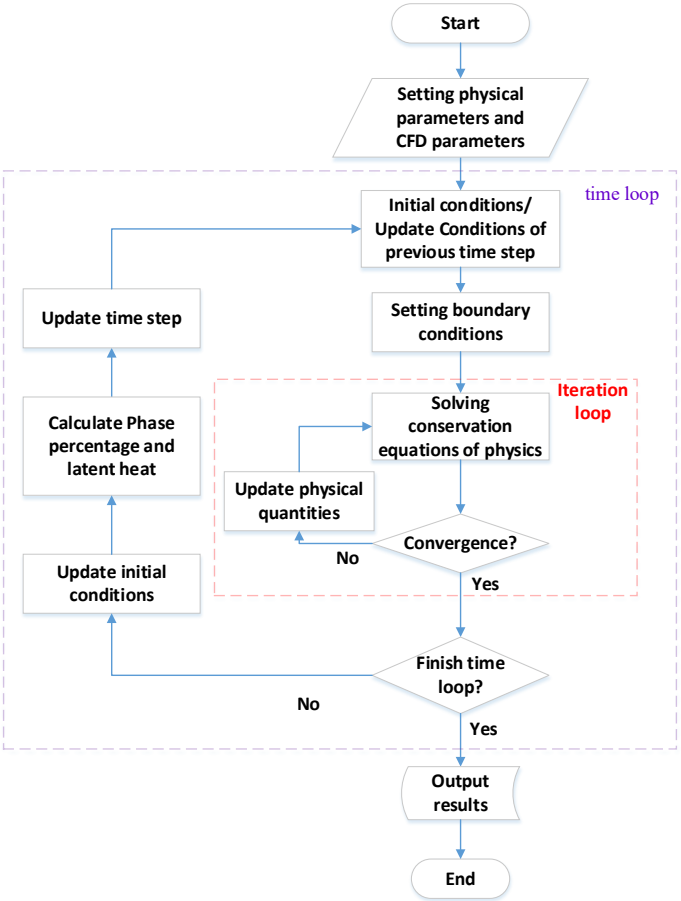

Fig.3. The flowchart of CFD with microstructure simulation.

the time loop. Using an external phase transformation program, the phase fraction X_i and the released heat Q of each phase are calculated. The heat Q is then fed back into the energy equation of the CFD for continued solving, achieving a coupled solution of phase transformation and flow field.

3. EXPERIMENT METHOD

To verify the simulation results through experiment, the Φ5.5mm wire rod of alloy steel was cut into 14cm round bars. A hole with a diameter of Φ2.0mm and a depth of 7.0cm was drilled to embed a Φ1.6mm fiberglass-coated K-type thermocouple, as shown in Fig.4. and Fig.5. Based on an on-site cooling speed of 15 mpm and a temperature drop of 200℃, the cooling rate was estimated to be approximately 0.56 (℃/S). The experimental process for verifying the simulation tool involved heating the wire rod in a laboratory furnace (as shown in Fig.6) to 870℃ (with A3 around 841℃), then cooling it at different rates while tracking the temperature history (Fig.7). The simulation was verified through temperature measurements and metallographic results.

Fig.4. The photo of the rod with a hole.

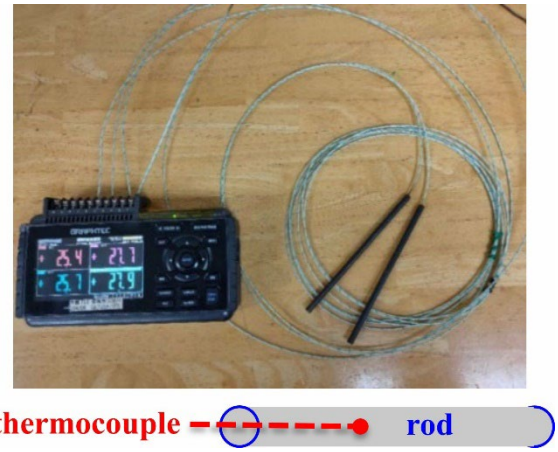

Fig.5. The photo of the rod with an inserted thermocouple.

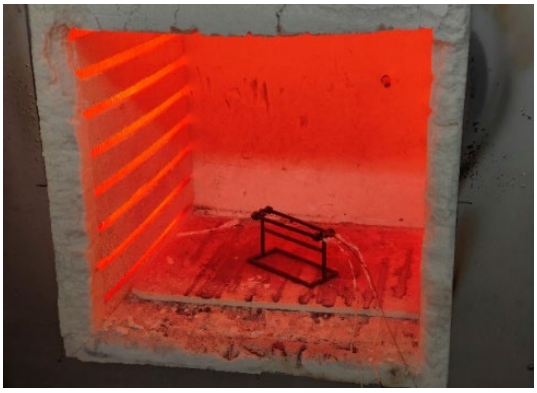

Fig.6. The photo of the support and the rod inside the experimental furnace.

Fig.7. The photo of the experimental system.

4. RESULTS AND DISCUSSION

Adjusting the simulation parameters for austenite grain size shows that a 4 μm grain size matches the cooling process with the experimental results, as shown in Fig.8. and Fig.9. The simulation's temperature progression aligns with the experimental results at the phase transition points. However, discrepancies in the simulated latent heat result in differences in temperature rise. The maximum error is about 3%. The metallographic comparisons show that the simulated pearlite content is about 52.5% and close to the experimental result of 55% at a cooling rate of 0.1 ℃/s (Fig.10). Additionally, the perlite proportions in the experiment and simulation are 71% and 76.3% respectively at the cooling rate of 0.6

(℃/S) as shown in Fig.11. The trends of temperature profile and microstructure percentage in the experiment and simulation are consistent, which provide that the CFD meets the requirements for engineering applications.

The transient temperature results of the coils under the insulation cover during cooling are shown in Fig.12. Through CFD simulation, the temperature distribution of the inner wall of the cover, the furnace rollers, and the coils were determined. The results show that the side part of the coils are high-temperature area. Due to the existence of a heat source, the temperature of the nearby

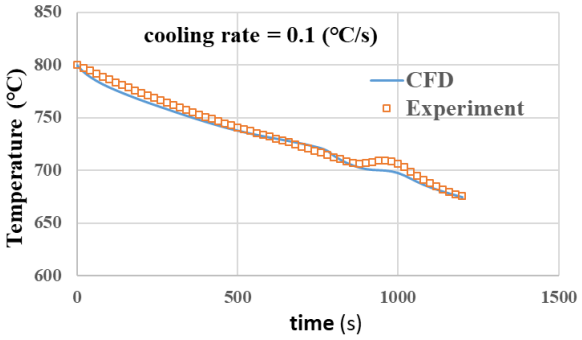

Fig.8. Comparison of the temperature histories between the experiment and CFD under a cooling rate of 0.1 (℃/s).

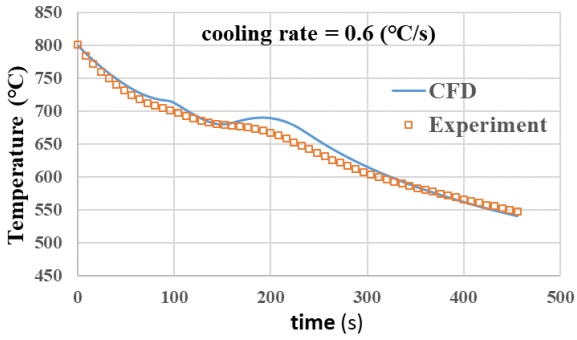

Fig.9. Comparison of the temperature histories between the experiment and CFD under a cooling rate of 0.6 (℃/s).

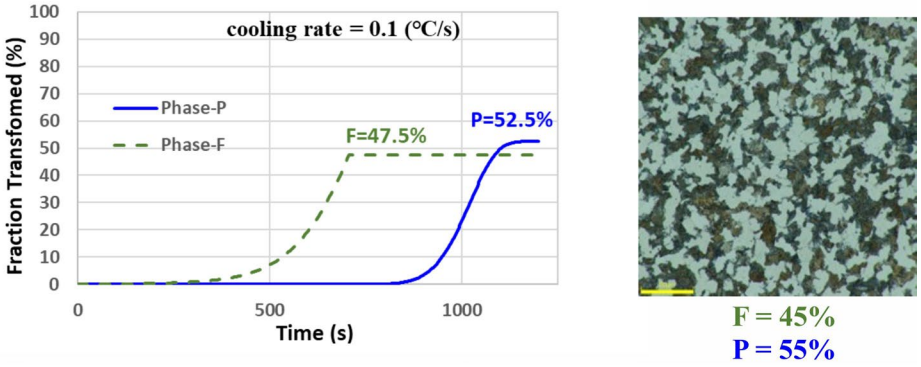

Fig.10. Simulated microstructure proportions (left image) and experimental microstructure proportions (right image) under a cooling rate of 0.1 (℃/S).

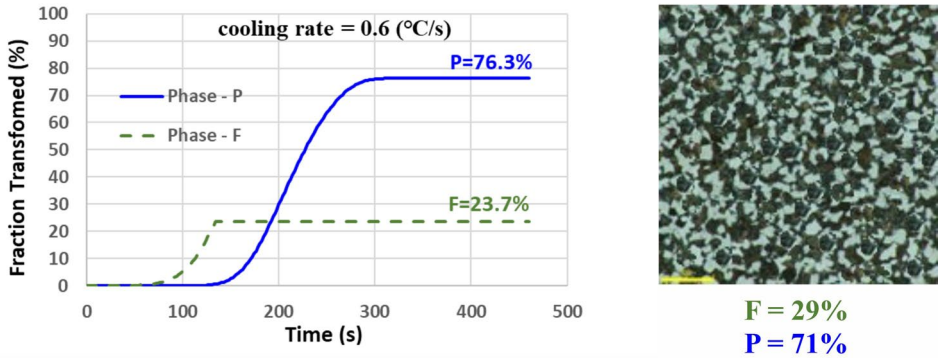

Fig.11. Simulated microstructure proportions (left image) and experimental microstructure proportions (right image) under a cooling rate of 0.6 (℃/S).

wall and furnace rollers is higher than in other areas. This also slows down the temperature decrease on the side part of the coils. Conversely, the center part of the coils cools down more quickly due to better heat dissipation conditions, which results from its scattered placement.

The simulation results of temperature and mechanical properties (TS) after completion of phase transformation are shown in Fig.13. The temperature history is a key factor affecting mechanical properties. Furthermore, the temperature distribution at the end of cooling is still correlated with mechanical properties. It exhibits a trend where lower temperatures correspond to higher TS values. The axial TS distribution for the coils arranged in the middle is illustrated in Fig.14, showing a distribution where TS drops sharply from 880 MPa to below 800 MPa. The maximum ΔTS is almost 97 MPa. The simulated coils have fewer stacks and less mass compared to the actual ones, which results in smaller calculated temperature differences and ΔTS. However,

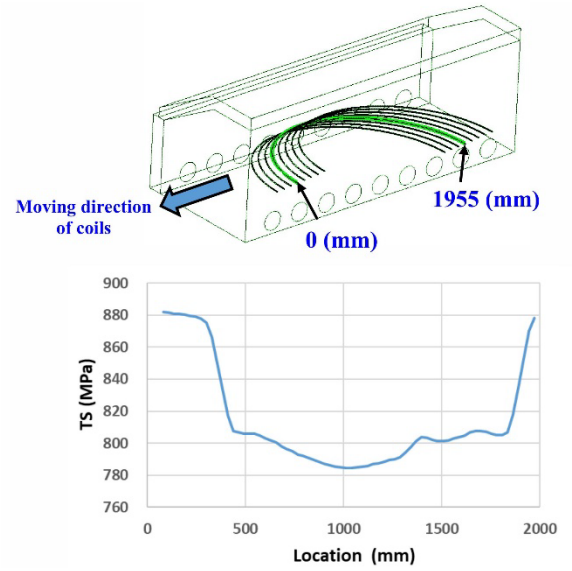

Fig.14. Simulation results of the TS distribution along the coil axis (green line of up sketch).

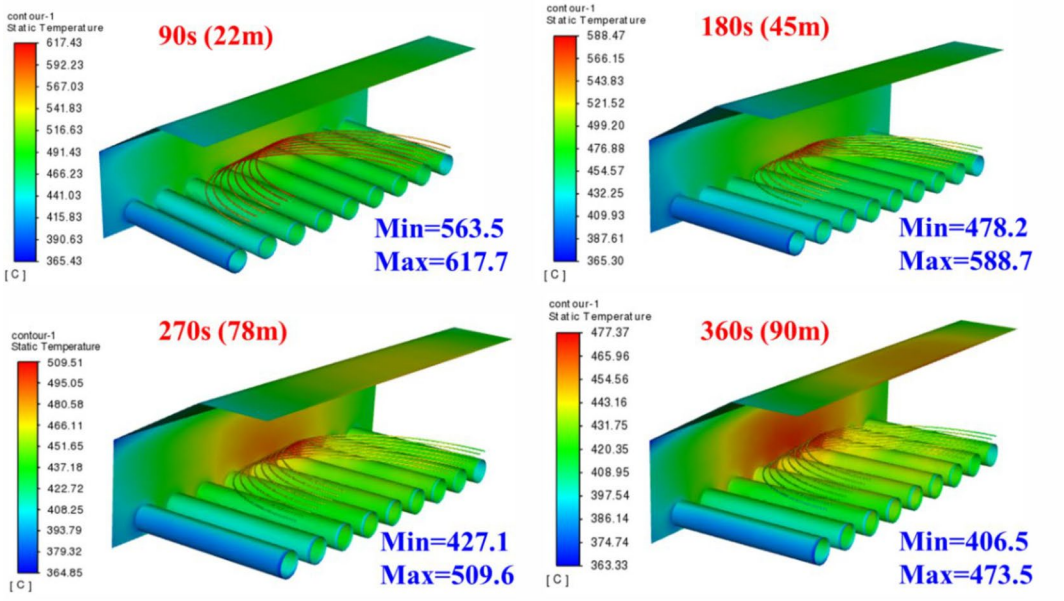

Fig.12. The transient results of temperature distribution from CFD.

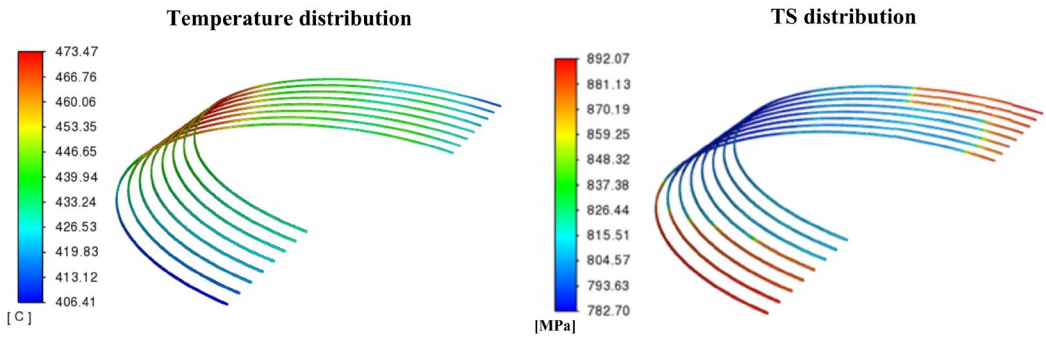

Fig.13. Simulation results of the coil at the end of cooling.

the trends and relative distributions of the physical quantities in the simulation are consistent with the actual results.

For quantitative analysis, the wire coils are divided into five equal parts in the study (Fig.15). Each part has an equal volume of wire representing the same initial total enthalpy. The equal surface area allows for comparative heat dissipation analysis. Analysis of the CFD results, the temperature profile (Fig.16.) shows that the phase transition occurs approximately in zone #2 to zone #4 corresponding to the actual production line. At the initial stage of cooling, the temperature difference between the center past and the side part gradually increases. During the phase transition period, the cold point heats up due to the early occurrence of the phase transition, which results in a temporary reduction of the temperature difference.

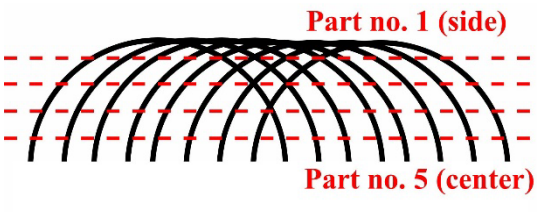

Fig.15. The diagram of the division zone for analyzing.

Fig.17. (left) shows the distribution of microstructural changes in the wire coil. The diagram indicates that the main microstructure at the side (dotted line) is pearlite (green dotted line) and it accounts for more than 90%. The side part just has a very small amount of ferrite. However, approximately 53% bainite (purple solid line) and about 40% pearlite (green solid line) are formed at the center part (solid line). The TS can be determined according to microstructure (as shown in Fig.17. right) and the calculated average TS difference reaches 67 MPa.

The analysis of the heat dissipation distribution during the cooling process at the center and side of the wire coil is shown in Fig.18. In the early stage of cooling, the heat transfer is large due to the significant temperature difference between the wire coil and the environment. As the temperature difference decreases, the heat transfer also decreases. However, the exothermic reaction in the phase transition region causes a slight increase in heat transfer. By integrating the total heat transfer, it is shown that the proportion of radiative heat to total heat transfer (R/T) is 75% at the center and 88% at the side. Since the center has a larger windward area, it has a higher proportion of convective heat transfer. The phase transition occurs in the latter part of zone #2, where the R/T ratio still exceeds 81%. Such a high percentage of

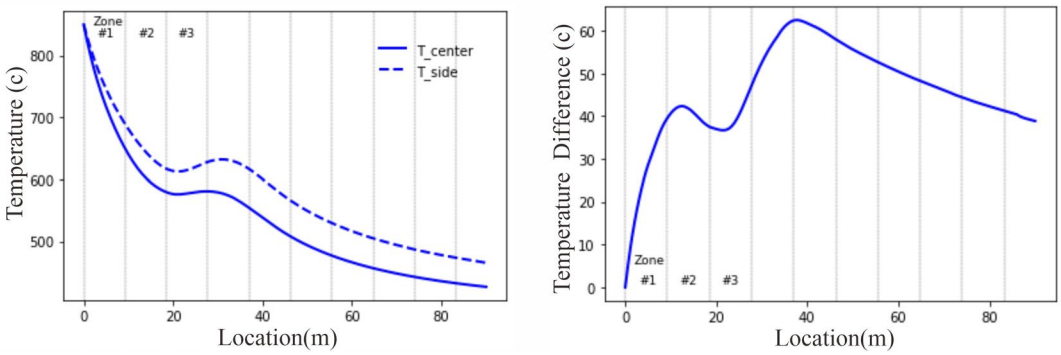

Fig.16. The temperature profiles of the center and side of the wire coil during cooling (left diagram) and the temperature difference distribution (right diagram).

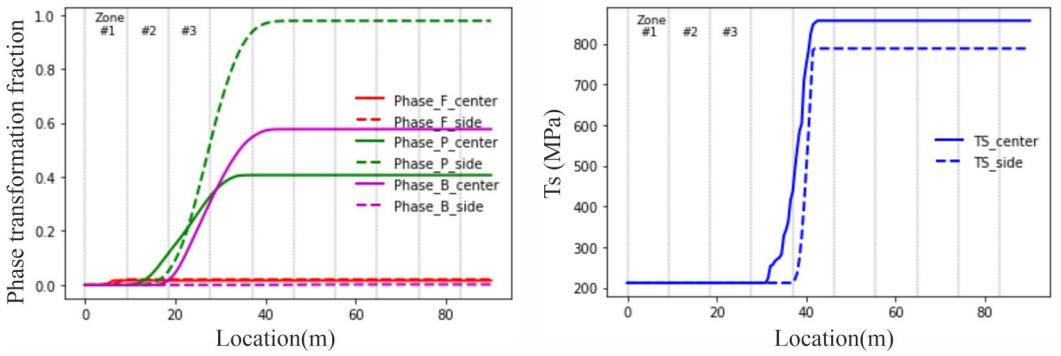

Fig.17. The microstructural distribution of the center and side of the wire coil (left diagram) and the TS distribution (right diagram).

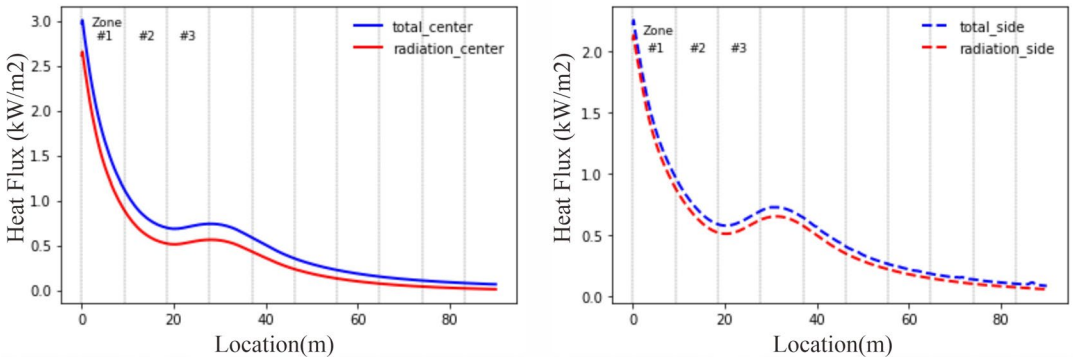

Fig.18. The diagram of total heat and radiative heat of rods over time (left diagram-center part; right diagram-side part).

R/T makes radiation the primary heat dissipation mechanism.

5. CONCLUSIONS

This study incorporated material microstructure changes and latent heat effects to establish a simulation tool for the slow cooling of wire coils with the cover. This tool was used to explore the impact of insulation covers on heat transfer in wire coils. The relevant conclusions are as follows:

1. The slow cooling experiments conducted with test rods validated the simulation tool. The maximum temperature history error is about 3%, meeting the requirements for engineering applications.
2. Simulating the axial distribution of TS in the wire coil, the maximum ΔTS reaches 97 MPa. Such a large TS difference is attributed to varying cooling rates between hot and cold spots, which aligns with practical observations.
3. The proportion of radiative heat to total heat transfer (R/T) was 75% at the center part and 88% at the side part of the coils respectively. The phase transition occurs in the latter part of zone #2, where the R/T ratio still exceeds 81%. Such a high percentage of R/T makes radiation the primary heat dissipation mechanism.

In the future, the developed simulation tool will be used to analyze variations of wire coil products in Stelmor and evaluate improvement plans to enhance production line processing capabilities.

REFERENCES

1. Monserrat Sofia Lopez-Cornejo et al., Numerical Simulation of Wire Rod Cooling in Eutectoid Steel under Forced-Convection, Metals, vol. 11, 2021.
2. Michal Piwowarczyk et al., Phase transformation model for adjusting the cooling conditions in Stelmor process to obtain the targeted structure of thermomechanically rolled wire rod used for fastener production, Metallurgical Research & Technology, vol. 119, 2022.
3. Jun-kai Huang et al., Effect of controlled cold air distribution on temperature profile and phase transformation of wire loops in the Stelmor air-cooling process, Applied Thermal Engineering, vol. 143, 2018, pp. 311-320.
4. Jun-kai Huang et al., Effect of Ring Configuration on the Deviation in Cooling Rate and Mechanical Properties of a Wire Rod during the Stelmor Cooling Process, Journal of Materials Engineering and Performance, vol. 29, 2020, pp. 1732-1740.
5. Zhang Jun, Sun Zhenlong, Current Status and Optimization of the Stelmor Cooling Process, China Equipment Engineering, 2011, pp. 36-38.
6. Jun-kai Huang et al., Effects of nozzle shape and arrangement on the cooling performance of steel wire rod in the Stelmor cooling process, Applied Thermal Engineering, vol. 164, 2020.
7. Hu Xiaodong et al., High-speed Wire Rod Mill Stelmor Line Air-mist Cooling Device and Method, CN1287921C, 2004.
8. Zhang Chi et al., High-speed Wire Rod Mill Stelmor Line Cooling Method and Cooling Device, CN101480669B, 2008.
9. Zhou Min et al., A High-efficiency Air Cooling Device, CN105522008B, 2016.
10. Jun-kai Huang et al., A three-dimensional mathematical model to predict air-cooling flow and temperature distribution of wire loops in the Stelmor air-cooling system, Applied Thermal Engineering, vol. 116, 2018.
11. Suncana S.H. et al., Prediction of Microstructure Constituents' Hardness after the Isothermal Decomposition of Austenite, Metals, Vol. 11, 2021.